

# Seismic Performance of Cementitious Grout Filled Coupler and Sleeve Connections in Precast Wall Panels under Cyclic Lateral Loading

Joyson Silva PARISUTHAM<sup>1\*</sup>, Jaya KRISHNAN PRABHAKARAN<sup>2</sup>, Binu SUKUMAR<sup>1</sup>

<sup>1</sup> Department of Civil Engineering, R.M.K. Engineering College, Gummidipoondi, Tamilnadu 601206, India

<sup>2</sup> Structural Engineering Division, Department of Civil Engineering, Anna University, Chennai 600025, India

<http://doi.org/10.5755/j02.ms.33883>

Received 19 April 2023; accepted 13 June 2023

This study investigated the seismic performance of cementitious grout filled coupler and sleeve connections in precast wall panels under cyclic lateral loading. The effectiveness of these connections in enhancing the seismic performance of precast concrete walls was evaluated. In many countries, grouted coupler connections are the preferred option, whereas sleeve connections were more commonly utilized in India due to the belief that a greater portion of the dowel being grouted enhances structural stability. Tests were conducted on full scale precast wall panels to study the behaviour of connections by applying a displacement-controlled cyclic lateral loading and the results were discussed. The experimental study revealed that the cementitious grout filled coupler connection exhibited better seismic performance and was recommended for precast wall panel connections over the grouted sleeve connection. Compared to the grout filled sleeve connection, the specimen with an unbonded segment demonstrated an 8% rise in energy dissipation, while the specimen with a grouted coupler connection displayed a 55 % increase.

*Keywords:* precast wall panel connections, cyclic lateral loading, seismic performance, cementitious grout filled coupler and sleeve connections.

## 1. INTRODUCTION

Precast construction is becoming an emerging construction practice in many parts of the world to meet the requirements of the construction industry in terms of time and quality. Typically, it involves mass production of repetitive elements of the same type in standard sizes. Precast concrete has many advantages over conventional cast in situ concrete in terms of more sustainable construction methods, improved quality control, quick construction, and reduced construction cost. However, designing of connection is one of the major challenges for the successful construction of precast reinforced concrete structures [1]. The connection configuration affects the constructability, strength, stability, flexibility and redistribution of loads when the structure is subjected to loading [2]. When these precast structures are constructed in high seismic intensity regions, the safety of the structure becomes a major concern due to the joint failure of connections.

Numerous studies have highlighted the challenges associated with integrating connections in precast structures, which can be addressed by improving serviceability through increased ductility and redundancy [3]. In the context of shear walls, the most commonly adopted connections are unbonded post-tensioned connections, bolted connections, and grouted connections [4]. The failure pattern observed in the specimens subjected to cyclic loading was the crushing and spalling of the dry pack grout. Experimental research conducted by Soudki et al. [5] on various horizontal connections with mild steel dowel bars, shear keys, and post-tensioning strands and rods

found that the observed mode of failure in all specimens under cyclic loading was due to the crushing and spalling of the dry pack grout. Grouted shear keys increased the shear resistance to a certain level and limited horizontal slip. The confinement provided by the sleeves increased the compressive strength of the grout their contribution to the seismic performance of precast concrete elements. Bulent Erkmen et al. [6] investigated the self-centering behavior of unbonded, post-tensioned precast concrete shear walls under cyclic loading and concluded that the post-tensioning force and axial load applied had negligible effects on self-centering behavior. Belleri et al. [7] explored grouted sleeve connections for a column to foundation connections of precast concrete structures in seismic regions, demonstrating that grouted sleeves ensured similar ductility and energy dissipation capacity of structural members. The compressive strength of the grout was also increased by the sleeves' confinement. Yajun et al. [8] tested pre-cast shear walls to evaluate the feasibility of a restraint grout splicing method that uses spiral reinforcements. The specimens were tested until they failed by leading to large deformation or the lateral load resistance of the specimen reduced to 85% of the lateral bearing capacity. The test results showed that the specimen with less splicing length offered less stiffness as displacement increased, but still satisfied codal provisions. The confinement provided for the grout by means of pipe and corrugated sleeve showed comparable differences in the energy dissipation capacity. Peng et al. [9] proposed a new method for connecting steel bars in precast shear wall panels with a steel sleeve having an infusion pipe and a checking pipe that could later be filled with mortar. The test results showed that the mortar-sleeve connection effectively

\* Corresponding author. Tel.: +91 9042680804.  
E-mail: [jsp.civil@rmkec.ac.in](mailto:jsp.civil@rmkec.ac.in) (J. S. Parisutham)

transferred stresses on the vertical steel bars. Sun et al. [10] developed a connection method for shear wall panels to form a stable and reliable load transferring system using a dry connection with horizontal steel connectors and high-strength bolts. However, the friction mechanism provided in this connection was insufficient in providing the necessary load transfer when the bolt diameter and pre-tensioning force were smaller. Elsayed et al. [11] studied grouted dowel specimens with different embedded lengths under unidirectional excitation and found that the load carrying capacity was nearly identical in all the tested cases and was not affected by the difference in embedded length. The provision of an unbonded segment also shows significance in improving the energy dissipation capacity. Sun et al. [12] investigated the behavior of rabbet-unbonded connections under cyclic quasi-static loading and found that the energy dissipation capacity and ductility were notably enhanced by the presence of an unbonded segment.

Several studies were conducted to evaluate the performance of cementitious grouted sleeve and coupler connections in precast construction. Most of these studies have focused on the ultimate strength of the connections and their ability to resist monotonic loads. However, the seismic performance of these connections, which is critical for earthquake-prone regions, has not been adequately explored. In this study, the behavior of three different connections was studied under reverse cyclic loading. This investigation aims to determine which connection type performs better in terms of seismic performance.

## 2. EXPERIMENTAL STUDY

### 2.1. Overview

A ten-story precast building situated in Chennai has been selected for the present study and the analysis has been carried out using ETABS Software. The structure has been analyzed for 14 different load combinations as per the IS 1893 Part: 1, 2002. The critical design forces, including shear force, bending moment, and axial load, have been extracted from the analysis and are listed as follows: 57.52 kN of shear force, 3730.5 kNm of bending moment, and 935.53 kN of axial load. The design and detailing of the wall panels were done as per IS 1893 and IS 13920 provisions. The 3-Dimensional view of the ETab Software Model is shown in Fig. 1.

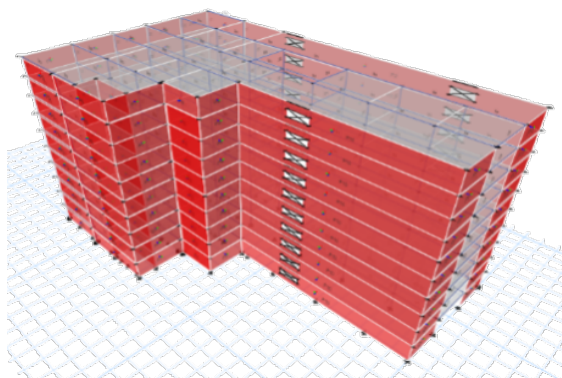


Fig. 1. 3-Dimensional view of the ETab software model

### 2.2. Material properties

M30 grade ready mix concrete and Fe500 grade reinforcement bars were used for preparing all the specimens. The mean compressive strength of three 150 mm × 150 mm × 150 mm cubes was found to be 34.89 MPa and the test results are given the Table 1.

Table 1. Compressive strength of concrete

Specimen number	Ultimate load, kN	Compressive strength, MPa	Average compressive strength, MPa
1	715	31.77	34.89
2	872	38.75	
3	769	34.17	

Commercially available non-shrinking and flowable grout were used in the joint region. The mean compressive strength of the grout in 2 days and 28 days were 43 MPa and 67.15 MPa respectively and the test results were given in Table 2. Similarly, reinforcement samples from different diameter bars were tested to ensure their specified yield strength.

Table 2. Compressive strength of cementitious grout

Specimen number	2 Days		28 Days	
	Compressive strength, MPa	Average	Compressive strength, MPa	Average
1	45	43	66.36	67.15
2	41		67.34	
3	44		67.75	

### 2.3. Specimen details

To investigate the behaviour of wall panel connections subjected to lateral reverse cyclic loading, three specimens were fabricated. The specimens were 1200 mm wide, 850 mm tall, and 150 mm thick. The dowel connection was designed to resist the shear force acting at the connection region [13]. The specimens were provided with two layers of reinforcements and edge reinforcements were also provided. The reinforcement detailing diagram is shown in Fig. 9, Fig. 10. The reinforcement detailing was the same for all the specimens except the dowel portion. The coupler used in the present study and the specimens are shown in Fig. 2 to Fig. 6.



Fig. 2. Grouted coupler (source: dextra coupler)

In the case of specimen S3, to achieve the unbonded segment, the top and bottom panels were interchanged and the grout is filled in the bottom panel, only up to the required portion leaving the top 300 mm unbonded. Holes were made at the required locations on the front face of the bottom panel so that excess grout beyond that point came out and

the length of the unbonded segment was maintained. A gap of 20 mm was maintained with the help of a metal shim pad and a grout layer of 20 mm thickness was provided in between the top and bottom panels to create a better bonding. The specimen details are given in Table 3.

**Table 3.** Specimen details

No.	Specimen name	Connection type	Diameter of the dowel bar, $\phi$	Length of the dowel portion
1	S1	Grouted sleeve	16 mm	$50\phi = 800$ mm
2	S2	Grouted coupler	16 mm	155 mm
3	S3	Grouted sleeve with unbonded segment	16 mm	$50\phi = 800$ mm in which 300 mm is left unbonded



**Fig. 3.** Wall panel with protruding dowel bars



**Fig. 4.** Wall panel with grout sleeve



**Fig. 5.** Grouted coupler with connecting rod

## 2.4. Instrumentation

The wall panels were instrumented in such a way that the strain in the bars and lateral displacement of the wall

panel are recorded properly when the panels were tested for lateral reverse cyclic loading under the constant axial load. In a single specimen, the upper wall panel and the lower wall panels were provided with four separate strain gauges to measure the strains in the bars and strains in the duct or coupler.



**Fig. 6.** Wall panel with protruding bars for coupler

To measure the displacement of the top panel, an LVDT fixed on the opposite side of the lateral loading point is employed at the top of the panel. The Schematic of the Loading setup with S1 type specimen is shown in Fig. 7 and Fig. 11 show the experimental setup in the lab.

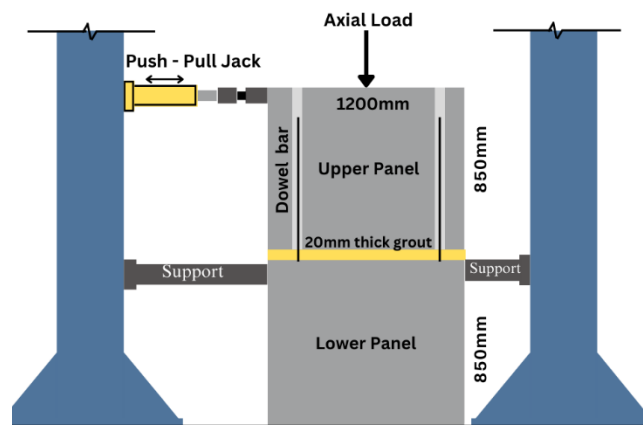


**Fig. 7.** Schematic of the loading setup with S1 type specimen

## 2.5. Loading pattern

The testing has been done using displacement-controlled testing protocol. The loading protocol used here is finalized based on ACI T1.1 R-01 provisions [14]. An axial load of 1 %  $A_g \cdot f_{ck}$  is maintained throughout the test for all three specimens [15]. A manually operated, 200 kN push-pull hydraulic jack was used to apply cyclic load. The jack is linked to the loading frame on one end and to the top of the wall panel via a pinned-type connection and a calibrated load cell on the other end. Three repeated cycles were applied in each magnitude level and the cycle drift ratios were finalized in such a way that the value is more than 1.25 times and less than 1.5 times the previous drift ratio [16]. The selected drift ratios are 0.2, 0.3, 0.5, 0.75, 1, 1.25, 1.5, 2.25, 2.5, 3.375 and 3.5. The displacement-controlled loading protocol calculated based on the drift ratios is shown in Fig. 8. The test was carried out till there

was a reduction of 15 to 20 percent in the maximum loading capacity [8, 15, 17].

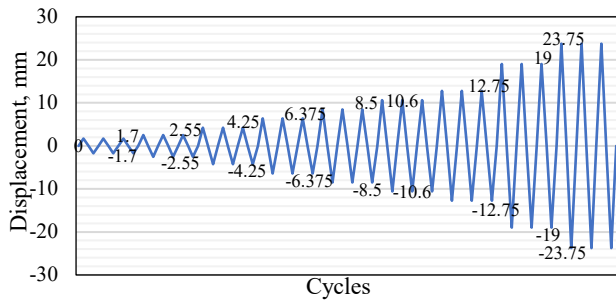


Fig. 8. Loading protocol followed

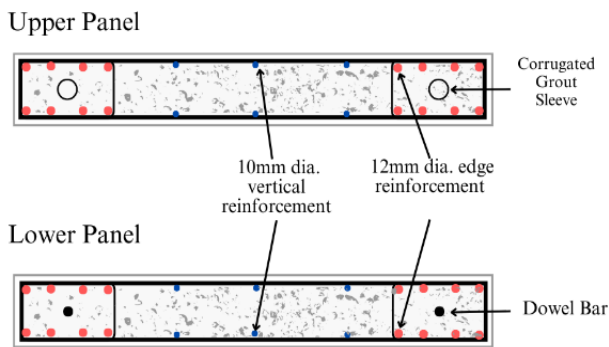


Fig. 9. Reinforcement details of specimens S1 and S3

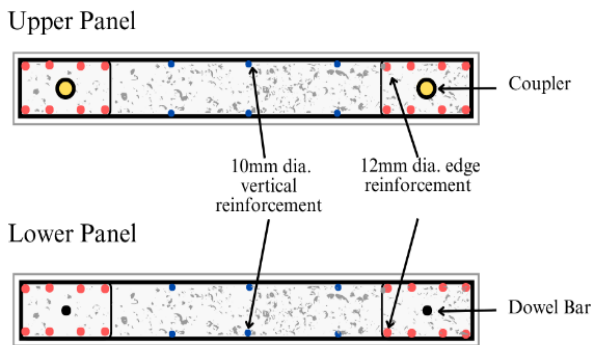


Fig. 10. Reinforcement details of specimen S2

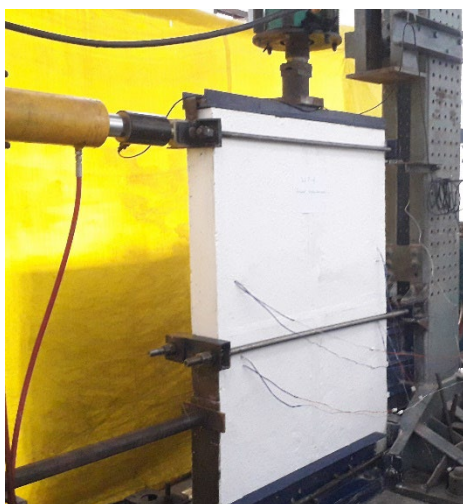


Fig. 11. Lateral loading test setup in the lab

### 3. RESULTS AND DISCUSSION

#### 3.1. Hysteresis behaviour and skeleton curves

The displacement-controlled load was applied at the top of the upper panel and the load resisted by the panel is measured on the opposite face. During the initial phases, a single horizontal crack emerged on the 20 mm grout layer that was placed between the wall panels. As loading continued, additional cracks were formed and eventually merged to create a bigger and more widespread crack [5]. Fig. 12 and Fig. 13 shows the tested specimens with cracks in the grout layer.

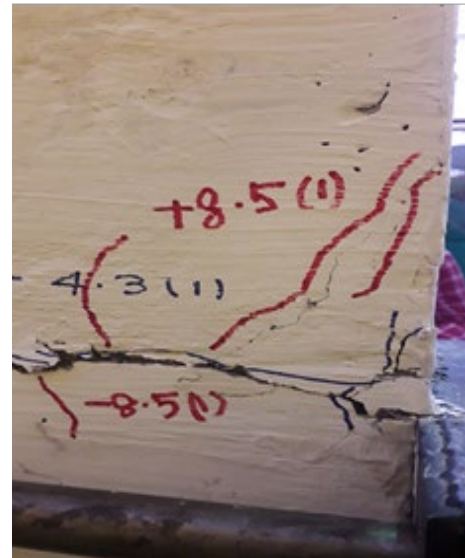


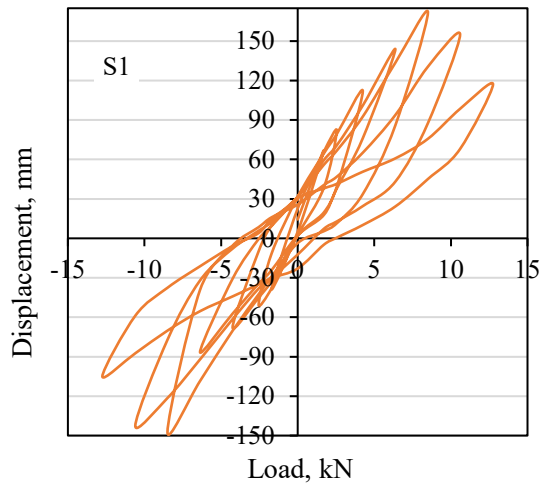
Fig. 12. Crack patterns observed



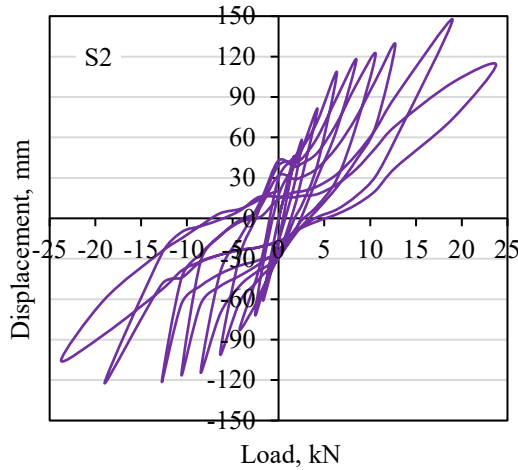
Fig. 13. Crack patterns observed

The relationship between the lateral load and displacement is given in Fig. 14 a–c. The specimen S1 reached the maximum lateral load capacity of 171.78 kN when the drift ratio was 1 and then in the next cycle, it decreased by 9.76 % and in the next consecutive cycle it decreased by 32 %, so the test has been stopped. In the specimen S2 with the grouted coupler, the maximum load was 147.36 kN when the drift ratio was 2.25.

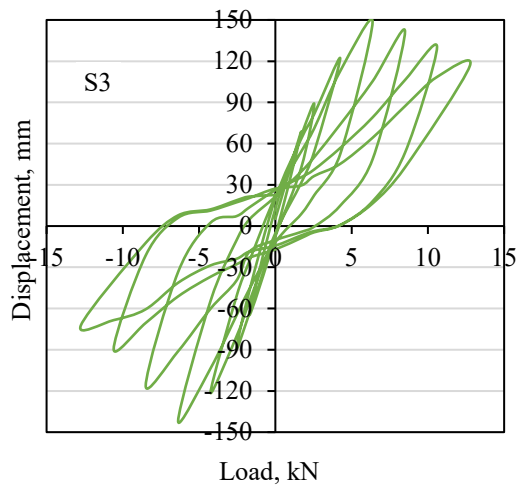
When the strength got reduced by 22.69 % at the drift ratio of 2.8, the test has been stopped. Similarly, in the third specimen S3, the drift ratio was 0.75 when the maximum load reached 148.64 kN, and the test was continued till there was a reduction of 21.62 % at the drift ratio of 1.5.



a



b



c

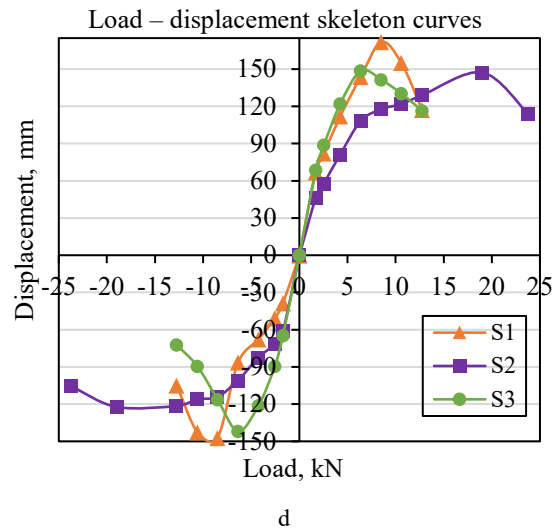


**Fig. 14.** a – load-displacement relationship curve of grouted sleeve connection; b – load-displacement relationship curve of grouted coupler connection; c – load-displacement relationship curve of grouted sleeve connection with unbonded segment; d – load-displacement relationship skeleton curves of all the three specimens

The difference in the drift ratios is due to the difference in the amount of energy dissipation capacity of the connections adopted. The envelope curves of hysteretic curves obtained from the load-displacement curves of all three experiments are given in Fig. 14 d. Compared to the S1 and S3, the specimen S2 curve covers the larger portion of the plot since it has taken more drift to reach the maximum load. The load carrying capacity of specimen S1 was slightly higher than the other two specimens at the ultimate load. As the displacement increased beyond the ultimate load, the lateral load values started decreasing in all three specimens. The load carrying capacity of specimen S3 with an unbonded segment was lower than that of the normal grouted sleeve connection specimen S1, mainly due to the cavity maintained inside the sleeve. When compared to specimen S2, there was not much difference in the load carrying capacity of specimen S3, and it is almost the same in specimens S2 and S3.

### 3.2. Energy dissipation capacity and damping coefficient

The ability of a connection to dissipate energy when exposed to a lateral force is quantified by its energy dissipation capacity. The energy dissipation capacity was calculated for each loading cycle and the calculated cumulative energy dissipation capacity ( $E$ ) is given in Table 4 for all three specimens.

**Table 4.** Cumulative energy dissipation capacity and damping coefficient values

Specimen	Cumulative energy dissipation capacity $E$ , kNmm	Damping coefficient, $h_e$	$h_{ei}/h_e$
1	3245.88	0.6015	1.00
2	5048.22	0.7052	1.17
3	3510.33	0.6197	1.03

By calculating the area under each cycle of the load-displacement curve, the energy dissipated during every displacement cycle is determined, and the cumulative energy dissipation is then calculated. Fig. 15 shows how to calculate the energy dissipation capacity and the values are listed in Table 4.

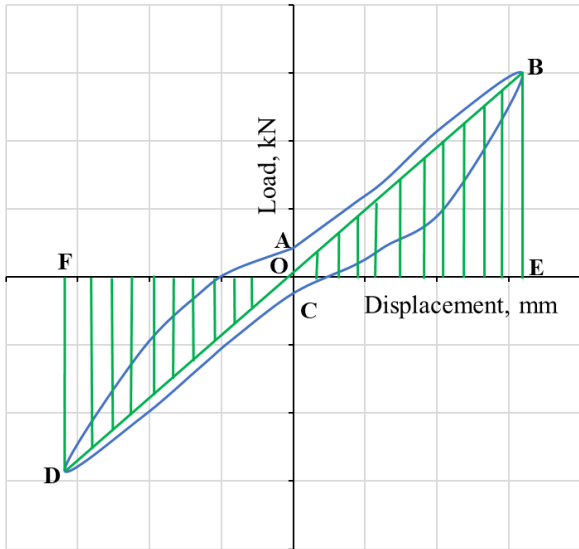


Fig. 15. Definition of the damping coefficient

Using the calculated energy dissipation value, the damping coefficient  $h_e$  was calculated using Eq. 1 given below. When comparing the energy dissipation capacity values, the specimen with an unbonded segment showed only an 8% increase than to S1 specimen with grouted sleeve connection but the specimen S2 with a grouted coupler connection showed a 55 % increase compared to the S1 specimen with a grouted sleeve connection. The comparison of cumulative energy dissipation and damping coefficient is shown in the Fig. 16, Fig. 17, Fig. 18.

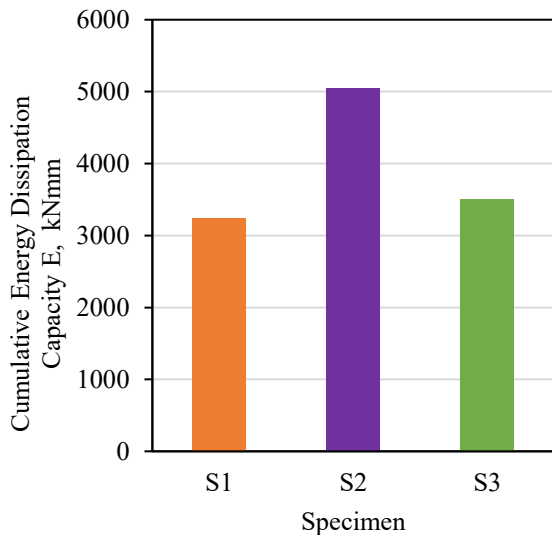


Fig. 16. Cumulative energy dissipation of specimens

$$\text{Damping coefficient } h_e = \frac{1}{2\pi} \times \frac{\text{Area of (ABCD)}}{\text{Area of (OBE)} + \text{Area of (ODF)}} \quad (1)$$

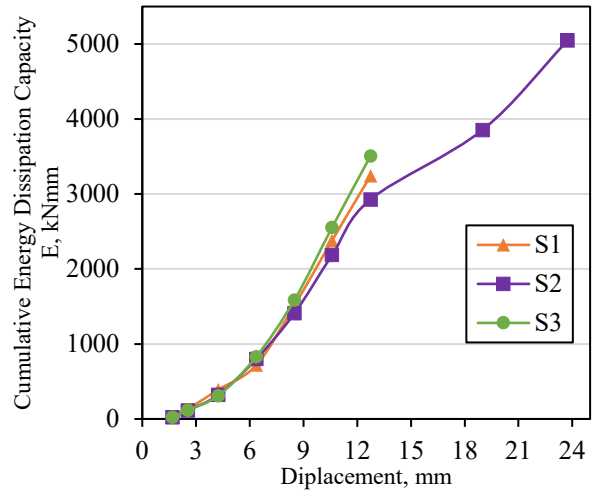


Fig. 17. Energy dissipation per cycle

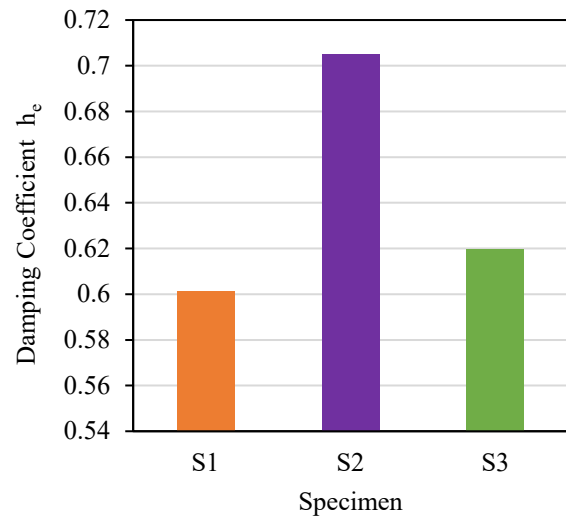


Fig. 18. Damping coefficient of specimens

### 3.3. Displacement ductility factor

The displacement ductility factor, a crucial parameter for assessing the seismic performance of structural connections, is defined as the ratio of lateral displacement  $\Delta_u$  to yield displacement  $\Delta_y$ .

The value of  $\Delta_u$  is determined by taking 85 % of the ultimate force, as reported by previous studies [18, 19, 20], whereas  $\Delta_y$  is obtained by measuring the displacement at 0.75 of the ultimate lateral displacement and multiplying it by 1.33, as per the definition given by R. Park [21]. A clear illustration of these definitions is presented in Fig. 19. The experimental results indicate that specimen S2 exhibits higher ductility than both the unbonded and normal grouted sleeve connections. Additionally, the damping coefficient of S2 was 1.5 times higher than that of S3 and 2.5 times higher than that of S1. The calculated displacement ductility factor values demonstrated that connection S2 shows a fully ductile response ( $> 3.5$ ), whereas the other connections exhibited restricted ductile behavior [22]. The calculated displacement ductility factors are shown in Table 5 and Fig. 20.

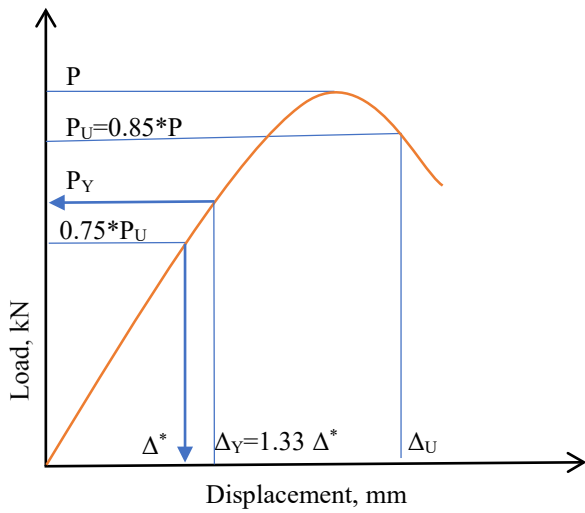


Fig. 19. Evaluation of ductility

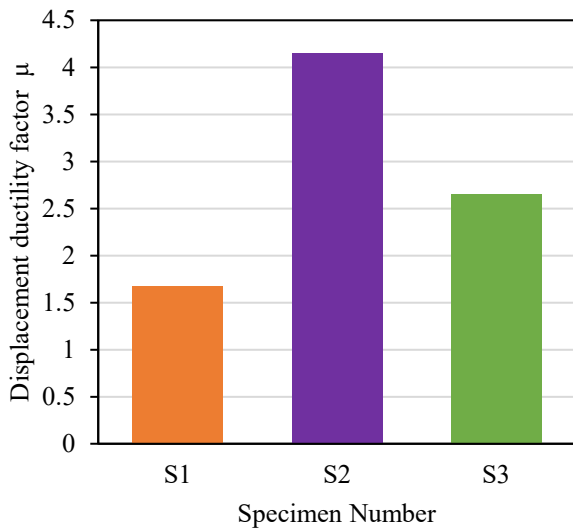


Fig. 20. Displacement ductility of specimens

Table 5. Displacement ductility values

No.	$\Delta_y$ , mm		$\Delta_u$ , mm		$\mu = \Delta_u/\Delta_y$		Average $\mu = \Delta_u/\Delta_y$
	+ve	-ve	+ve	-ve	+ve	-ve	
1	5.47	8.82	11.11	11.58	2.03	1.31	1.67
2	6.8	4.7	22.14	24.19	3.17	5.14	4.16
3	3.8	3.458	11.21	8.133	2.95	2.35	2.65

### 3.4. Stiffness degradation

In general, structural members will exhibit stiffness degradation when they are subjected to repeated cyclic loading. The reason for the stiffness degradation could be the loss of resistance offered by the connection due to cracking, yielding in the reinforcement bar, etc. The stiffness for every displacement level is determined by dividing the lateral load by the corresponding displacement. Fig. 21 shows how the stiffness values are decreasing with respect to the increasing displacement. In the positive direction, S1 and S3 offered more initial stiffness and in the negative direction, S2 and S3 offered more initial stiffness. The gradual decrease in stiffness shown in the S2 specimen

indicates that the grouted coupler connection is behaving in a better way than the other two specimens.

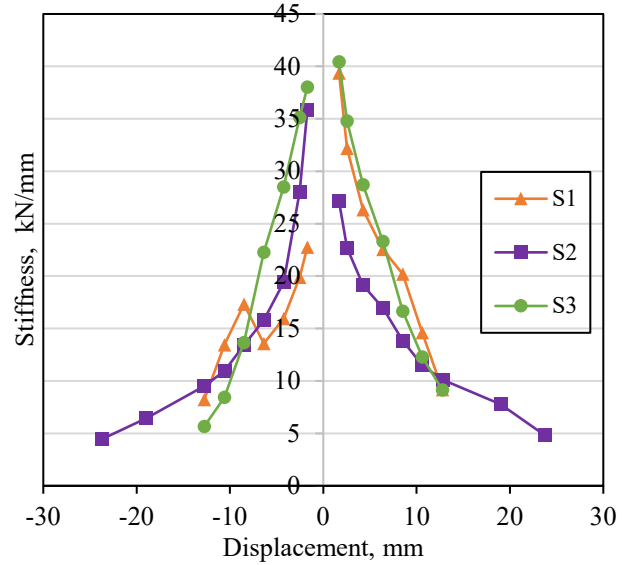


Fig. 21. Relation between stiffness degradation and lateral displacement

### 3.5. Load ratio

The load ratio is the average maximum load divided by the average yield load. The load ratios calculated for all three specimens at each displacement cycle listed in Table 6.

Table 6. Load ratio values

Displacement, mm	Specimen S1	Specimen S2	Specimen S3
	Load ratio		
1.7	0.52	0.63	0.72
2.55	0.66	0.76	0.97
4.25	0.89	0.96	1.32
6.375	1.14	1.22	1.57
8.5	1.57	1.35	1.4
10.6	1.47	1.39	1.19
12.75	1.1	1.46	1.02
19	–	1.57	–
23.75	–	1.28	–

In all the three specimens load ratio values are increasing up to the maximum lateral load point and after that it decreased slowly. In all three specimens the maximum load ratio was 1.57. The fact that the grouted coupler connection dissipated more energy than the other two connections despite having a lower load-resisting capacity suggests that it is better able to absorb and dissipate energy during a loading event. The relation between the load ratio and lateral displacement values are shown in Fig. 22.

## 4. CONCLUSIONS

From the experimental study conducted by applying reverse cyclic load on three different connections, the following conclusions are made.

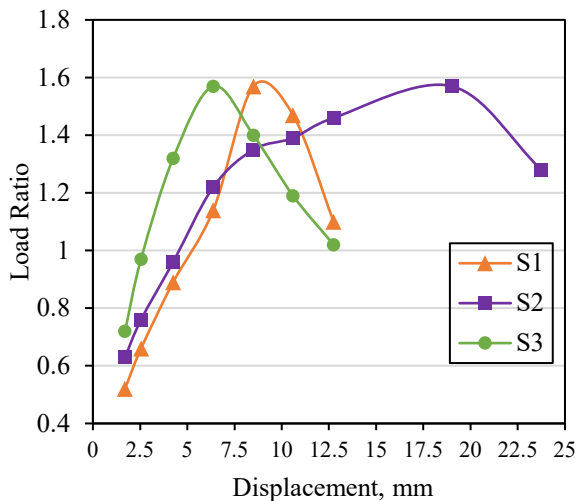


**Fig. 22.** Relation between the load ratio and lateral displacement

1. The cementitious grout filled coupler connection is found to be more effective than the grouted sleeve with unbonded segment and grouted sleeve connections in terms of energy dissipation capacity. The Specimen S2 with a grouted coupler connection showed a 55 % increase compared to the Specimen S1 with a grouted sleeve connection and it is confirmed that the grouted coupler connection will be the best option for precast connections in seismic regions.
2. The specimen with an unbonded segment showed an 8% increase in energy dissipation capacity than the Specimen S1 with grouted sleeve connection. The length of the unbonded segment along with the grout compressive strength has to be studied further to explore the possible advantages, and to find the optimum value of unbonded segment length.
3. Based on the observation and crack patterns, it is found that the thickness of the cementitious grout layer between the top and bottom panels has a major role in offering the initial resistance.
4. When compared with the loading ratio, all the specimens exhibited the same maximum loading ratio of 1.57, but the yielding started first in the grouted coupler connection than the other two connections. The fact that the grouted coupler connection dissipates more energy than the other two connections despite having a lower load-resisting capacity suggests that it is better able to absorb and dissipate energy during a loading event.
5. Further investigation is needed to determine the exact mechanisms by which the grouted coupler connection dissipates energy and to determine ways to improve the energy-dissipating capacity of the other two connections.

### Acknowledgments

The first author of this work thanks Anna University, Chennai and R.M.K. Engineering College, Chennai for the permission granted for his doctoral studies at Structural Engineering Division, CEG-Anna University, Chennai.

### REFERENCES

1. **Loo, Y., Yao, B. Z.** Static and Repeated Load Tests on Precast Concrete Beam-to-Column Connections *PCI Journal* 40 (2) 1995: pp. 106–115. <https://doi.org/10.15554/pcij.03011995.106.115>
2. **Stanton, J.F., Anderson, R.A., Dolan, C.W., McCleary, D.** Moment Resistant Connections and Simple Connections *PCI Journal* 32 (2) 1986: pp. 62–74. <https://doi.org/10.15554/pcij.03011987.62.74>
3. **Taheri, H., Hejazi, F., Vaghei, R., Jaafar, M.S., Ali, A.A.** New Precast Wall Connection Subjected to Rotational Loading *Periodica Polytechnica-Civil Engineering* 60 (4) 2016: pp. 547–560. <https://doi.org/10.3311/ppci.8545>
4. **Sørensen, J.G., Hoang, L.C., Olesen, J.F., Fischer, G.** Test and Analysis of a New Ductile Shear Connection Design for RC Shear Walls *Structural Concrete* 18 (1) 2017: pp. 189–204. <https://doi.org/10.1002/suco.201600056>
5. **Soudki, K., West, J.S., Rizkalla, S.H., Blackett, B.** Horizontal Connections for Precast Concrete Shear Wall Panels Under Cyclic Shear Loading *PCI Journal* 41 (3) 1996: pp. 64–80. <https://doi.org/10.15554/pcij.05011996.64.80>
6. **Erkmen, B., Schultz, A.E.** Self-Centering Behavior of Unbonded, Post-Tensioned Precast Concrete Shear Walls *Journal of Earthquake Engineering* 13 (7) 2009: pp. 1047–1064. <https://doi.org/10.1080/13632460902859136>
7. **Belleri, A., Riva, P.** Seismic Performance and Retrofit of Precast Concrete Grouted Sleeve Connections *PCI Journal* 57 (1) 2012: pp. 97–109. <https://doi.org/10.15554/pcij.01012012.97.109>
8. **Yajun, L., Naiyan, G.** Tests on Seismic Behavior of Pre-cast Shear Walls with Vertical Reinforcements Spliced by Two Different Grout Ways *The Open Civil Engineering Journal* 9 (1) 2015: pp. 382–387. <https://doi.org/10.2174/1874149501509010382>
9. **Peng, Y., Qian, J., Wang, Y.** Cyclic Performance of Precast Concrete Shear Walls with A Mortar-Sleeve Connection for Longitudinal Steel Bars *Materials and Structures* 49 (6) 2016: pp. 2455–2469. <https://doi.org/10.1617/s11527-015-0660-0>
10. **Sun, J., Qiu, H., Lu, Y.** Experimental Study and Associated Numerical Simulation of Horizontally Connected Precast Shear Wall Assembly *Structural Design of Tall and Special Buildings* 25 (13) 2016: pp. 659–678. <https://doi.org/10.1002/tal.1277>
11. **Elsayed, M.A., Ghrib, F., Nehdi, M.L.** Experimental and Analytical Study on Precast Concrete Dowel Connections Under Quasi-Static Loading *Construction and Building Materials* 168 2018: pp. 692–704. <https://doi.org/10.1016/j.conbuildmat.2018.02.140>
12. **Sun, C., Liang, S., Zhu, X., Li, H., Guo, J., Li, G., Song, Y., Wu, D.** Experimental Study and Numerical Simulation of Precast Shear Wall with Rabbit-Unbonded Horizontal Connection *International Journal of Concrete Structures and Materials* 14 (1) 2020: pp. 01–16. <https://doi.org/10.1186/s40069-019-0379-3>
13. **Elliott, K.S.** Precast Concrete Structures *CRC Press eBooks* 2016: pp. 229–268. <https://doi.org/10.1201/9781315370705>

14. **ACI T1.1R-01.** Commentary on Acceptance Criteria for Moment Frames Based on Structural Testing, *American Concrete Institute*.
15. **Seifi, P., Henry, R.C., Ingham, J.** In-plane Cyclic Testing of Precast Concrete Wall Panels with Grouted Metal Duct Base Connections *Engineering Structures* 184 2019: pp. 85–98. <https://doi.org/10.1016/j.engstruct.2019.01.079>
16. **Hawkins, N.** Acceptance Criteria for Special Precast Concrete Structural Walls Based on Validation Testing *PCI Journal* 49 (5) 2004: pp. 78–92. <https://doi.org/10.15554/pcij.09012004.78.92>
17. **Park, R.S.** Evaluation of Ductility of Structures and Structural Assemblages from Laboratory Testing *Bulletin of the New Zealand Society for Earthquake Engineering* 22 (3) 1989: pp. 155–166. <https://doi.org/10.5459/bnzsee.22.3.155-1666>
18. **Xu, G., Wang, Z., Wu, B., Bursi, O.S., Tan, X., Yang, Q., Wen, L.** Seismic Performance of Precast Shear Wall with Sleeves Connection Based on Experimental and Numerical Studies *Engineering Structures* 150 2017: pp. 346–358. <https://doi.org/10.1016/j.engstruct.2017.06.026>
19. **Park, R., Paulay, T.** Reinforced Concrete Structures. John Wiley & Sons, New York, NY, USA, 1975. <https://doi.org/10.1002/9780470172834>
20. **Hemamathi, L., Jaya, K.P.** Behaviour of Precast Column Foundation Connection under Reverse Cyclic Loading *Advances in Civil Engineering* 2021: pp. 1–17. <https://doi.org/10.1155/2021/6677007>
21. **Park, R.** Ductility Evaluation from Laboratory and Analytical Testing *Proceedings of the Ninth World Conference on Earthquake Engineering* 8 1988: pp. 605–616.
22. **Paulay, T., Priestly, M.J.N.** Seismic Design of Reinforced Concrete and Masonry Buildings. Wiley, India, 2013. <https://doi.org/10.1002/9780470172841>



© Parisutham et al. 2023 Open Access This article is distributed under the terms of the Creative Commons Attribution 4.0 International License (<http://creativecommons.org/licenses/by/4.0/>), which permits unrestricted use, distribution, and reproduction in any medium, provided you give appropriate credit to the original author(s) and the source, provide a link to the Creative Commons license, and indicate if changes were made.